Kinetically balanced Gaussian basis-set approach to relativistic Compton profiles of atoms

Prerit Jaiswal and Alok Shukla*
Physics Department, Indian Institute of Technology, Powai, Mumbai 400076, India
(Received 11 August 2006; revised manuscript received 18 December 2006; published 7 February 2007)

Atomic Compton profiles (CPs) are a very important property which provide us information about the momentum distribution of atomic electrons. Therefore, for CPs of heavy atoms, relativistic effects are expected to be important, warranting a relativistic treatment of the problem. In this paper, we present an efficient approach aimed at *ab initio* calculations of atomic CPs within a Dirac-Hartree-Fock (DHF) formalism, employing kinetically balanced Gaussian basis functions. The approach is used to compute the CPs of noble gases ranging from He to Rn, and the results have been compared to the experimental and other theoretical data, wherever possible. The influence of the quality of the basis set on the calculated CPs has also been systematically investigated.

DOI: 10.1103/PhysRevA.75.022504 PACS number(s): 31.30.Jv, 32.80.Cy, 31.10.+z, 31.15.−p

I. INTRODUCTION

Recent years have seen tremendous amount of progress in the field of relativistic electronic structure calculations of atoms and molecules using Dirac-equation-based approaches [1]. Particularly noteworthy are the advances made in the field of basis-set-based relativistic electronic-structure theory pioneered by Kim [2] and Kagawa [3]. Although, initially, the basis sets employed in the calculations were of the ordinary Slater-type [2,3], however, nowadays, the preferred basis functions are those which incorporate the so-called kinetic-balance condition between the large and the small component basis functions [4–6]. The most commonly used variety of such functions in relativistic electronic-structure calculations are the kinetically balanced Gaussian functions (KBGFs) which have not only been instrumental in avoiding the problem of "variational collapse," but have also allowed the import of efficient algorithms developed in basis-set-based nonrelativistic quantum chemistry. Using such basis functions, calculations are now routinely performed both at the mean-field Hartree-Fock [henceforth Dirac-Hartree-Fock (DHF)] level [7,8], as well as at the correlated level, employing methods such as the configuration-interaction (CI) approach, both for atoms [9] and molecules [10].

However, the progress in calculating wave functions and atomic energies using KGBFs has not been matched by the progress in computing expectation values corresponding to various physical quantities. For example, atomic Compton profiles (CPs) are a very important property which provide us information about the momentum distribution of atomic electrons, and help us in interpreting the x-ray Compton scattering data from atoms in the large momentum-transfer regime [11]. Compton profiles are also very useful in understanding the bonding properties, as one makes a transition from the atomic scale to the scale of condensed matter [11]. Indeed, the nonrelativistic Schrödinger equation-based calculations of CPs of atomic and molecular systems both within an *ab initio*, as well as model-potential based formalisms are quite well developed [11]. As recently demonstrated by us, and several other authors earlier on, such nonrelativistic *ab initio* calculations of CPs can also be performed on crystalline systems [12]. However, for systems involving heavy atoms, on intuitive grounds one expects that the relativistic effects will become quite important, thereby requiring a relativistic treatment of the problem [13]. A while back Mendelsohn *et al.* [14] and Bigss *et al.* [15] presented the first fully relativistic calculations of atomic CPs which were performed at the DHF level, employing a finite-difference-based numerical approach. Yet, since that time, there has been hardly any activity in the field, which is surprising given the fact that now relativistic electronic-structure calculations are routinely performed employing KBGF basis functions. Therefore, in this work, our aim is to report calculations of atomic CPs at the DHF level, employing a basis set composed of KBGFs. Our approach is based upon analytic formulas for the CP matrix elements with respect to a KBGF basis set, whose derivation is presented in the Appendix. The DHF calculations of atomic CPs are presented for the entire rare gas series (He to Rn), and our results are compared to experimental data, wherever available. Additionally, our results for Ar, Kr, Xe, and Rn are also compared to the DHF results of Mendelsohn *et al.* [14] and Bigss *et al.* [15], and excellent agreement is obtained between the two sets of calculations.

At this point we would like to clarify one important aspect related to the relativistic effects which our calculations are computing, in light of the fact that there have been several papers in the literature dealing with a relativistic treatment of Compton scattering of bound electrons [16–18]. Several authors have pointed out that for very large photon energies, a fully relativistic treatment, within the framework of quantum electrodynamics, of the Compton scattering from bound electrons is essential [13]. When such a treatment of the problem is performed, it is not clear whether the Compton scattering cross sections can be written in terms of Compton profiles [13,16–18]. Our work presented here, however, does not correspond to that regime of photon energies. What we mean by the relativistic effects here are the changes in the computed CPs because of a relativistic treatment of the bound electrons within a Dirac-Hamiltonian-based formalism. Thus, our calculations assume that the Compton scattering from atomic electrons can be described in terms of the CPs under the impulse approximation [19]. The electron mo-

*Electronic address: shukla@phy.iitb.ac.in

mentum densities needed to calculate the CPs, however, are computed from the Dirac orbitals of the atomic electrons. This approach is identical to the one adopted in the earlier DHF calculations [14,15].

The remainder of this paper is organized as follows. In Sec. II we present the basic theoretical formalism behind the present set of calculations. Next, in Sec. III we present and discuss the results of our calculations. Finally, in Sec. IV our conclusions, as well as possible future directions for further work are discussed. Additionally, in the Appendix we present the derivation of the closed-form formulas for CPs over KBGFs used in our calculations.

II. THEORY

Our theory is based upon the Dirac-Coulomb Hamiltonian

$$H = \sum_i [c\alpha_i \cdot \mathbf{p}_i + c^2(\beta_i - 1) + V_{\text{nuc}}(r_i)] + \sum_{i<j} \frac{1}{r_{ij}}, \quad (1)$$

where c is the speed of light, $\mathbf{p}$ is the momentum operator, $V_{\text{nuc}}(r)$ is the electron-nucleus interaction potential, indices i and j label the electrons of the atom, and r_{ij} is the distance between the ith and jth electrons. For $V_{\text{nuc}}(r)$ a spherical finite-nucleus approximation is employed, with the radius estimated as $2.2677 \times 10^{-5} A^{1/3}$, where A is the atomic mass number [7]. The Dirac matrices are chosen to be $\alpha = \begin{pmatrix} \mathbf{0} & \sigma \\ \sigma & \mathbf{0} \end{pmatrix}$ and $\beta = \begin{pmatrix} \mathbf{I} & \mathbf{0} \\ \mathbf{0} & -\mathbf{I} \end{pmatrix}$, where $\mathbf{0}$, $\mathbf{I}$, and σ represent the 2×2 null, identity, and Pauli matrices, respectively. Equation (1) is solved under the DHF approximation utilizing spherical symmetry with the orbitals of the form

$$\psi_{n\kappa m} = r^{-1} \begin{pmatrix} P_{n\kappa}(r)\chi_{\kappa m}(\theta,\phi) \\ iQ_{n\kappa}(r)\chi_{-\kappa m}(\theta,\phi) \end{pmatrix}, \quad (2)$$

where $P_{n\kappa}(r)$ and $Q_{n\kappa}(r)$ are the radial large and small components, and $\chi_{\kappa m}(\theta,\phi)$ is the two-component angular part composed of Clebsch-Gordon coefficients and spherical harmonics. In the basis-set approach adopted here, the radial parts of the wave function are expressed as linear combination of radial Gaussian type of functions

$$P_{n\kappa}(r) = \sum_i C^L_{\kappa i} g^L_{\kappa i}(r)$$

and

$$Q_{n\kappa}(r) = \sum_i C^S_{\kappa i} g^S_{\kappa i}(r),$$

where $C^L_{\kappa i}$ and $C^S_{\kappa i}$, are the expansion coefficients of the large and small component basis functions, respectively. The large-component basis function is given by

$$g^L_{\kappa i}(r) = N^L_{\kappa i} r^{n_\kappa} e^{-\alpha_i r^2}, \quad (3)$$

while the small-component basis function is obtained by the kinetic-balancing condition [6]

$$g^S_{\kappa i} = N^S_{\kappa i} \left(\frac{d}{dr} + \frac{\kappa}{r} \right) g^L_{\kappa i}(r). \quad (4)$$

Above n_κ is the principal quantum number associated with a symmetry species ($n_\kappa = 1,2,2,3,3,\ldots$, for symmetry species $s, p_{1/2}, p_{3/2}, d_{3/2}, d_{5/2}, \ldots$), α_i is the Gaussian exponent of the ith basis function, and $N^L_{\kappa i}$, $N^S_{\kappa i}$ are the normalization coefficients associated with the large and the small component basis functions, respectively.

Under the impulse approximation [19], the differential cross section of Compton scattering of x rays from many-electron systems is proportional to the Compton profile

$$J(q) = \int \int dp_x dp_y \rho(\mathbf{p}), \quad (5)$$

where $\rho(\mathbf{p})$ is the momentum distribution of the electrons before scattering and q is the component of the momentum of the electron along the scattering vector, assumed to be along the z direction. Under the mean-field DHF approximation, for a closed-shell atom, the expression for the CP reduces to

$$J(q) = \sum (2j_i + 1) J_{n_i\kappa_i}(q), \quad (6)$$

where j_i is the total angular momentum of the ith orbital while $J_{n_i\kappa_i}$ is the CP associated with it;

$$J_{n_i\kappa_i}(q) = \frac{1}{2} \int_q^\infty \{|P_{n_i\kappa_i}(p)|^2 + |Q_{n_i\kappa_i}(p)|^2\} p dp, \quad (7)$$

where $P_{n_i\kappa_i}(p)$ and $Q_{n_i\kappa_i}(p)$ are the Fourier transforms of the radial parts of the large and small components, respectively, of the ith occupied orbital [cf. Eq. (2)] and are defined as

$$P_{n_i\kappa_i}(p) = \frac{4\pi}{(2\pi)^{3/2}} \int_0^\infty r P_{n_i\kappa_i}(r) j_{l_A}(pr) dr, \quad (8)$$

$$Q_{n_i\kappa_i}(p) = \frac{4\pi}{(2\pi)^{3/2}} \int_0^\infty r Q_{n_i\kappa_i}(r) j_{l_B}(pr) dr, \quad (9)$$

where $j_{l_A}(pr)(j_{l_B}(pr))$ is the spherical Bessel function corresponding to the orbital angular momentum $l_A(l_B)$ of the large (small) component. Therefore, calculation of atomic CPs involves computation of two types of integrals: (i) radial Fourier transforms of Eqs. (8) and (9), and (ii) momentum integrals of the Fourier transformed orbitals in Eq. (7). When one solves the DHF equation for atoms using the finite-difference techniques, then, obviously the calculation of atomic CPs mandates that both these types of integrals be computed by means of numerical quadrature. However, for the basis-set-based approach adopted here, in order to facilitate rapid computation of atomic CPs, it is desirable to obtain closed-form expressions for both types of integrals with respect to the chosen basis functions. Indeed, we have managed to derive closed-form expressions for the atomic CPs with respect to the KBGFs, which can be easily computer implemented. It is easy to see that within a KBGF-based approach, the integral of Eq. (7) can be computed in terms of the following two types of integrals:

$$J^{L;\kappa}_{ij}(q) = \frac{1}{2} \int_q^\infty p g^L_{\kappa i}(p) g^L_{\kappa j}(p) dp,$$

$$J_{ij}^{S;\kappa}(q) = \frac{1}{2}\int_q^\infty p g_{\kappa i}^S(p) g_{\kappa j}^S(p) dp,$$

where $g_{\kappa i}^L(p)$ and $g_{\kappa i}^S(p)$ are the radial Fourier transforms [cf. Eqs. (8) and (9)] of the large and small component basis functions $g_{\kappa i}^L(r)$ and $g_{\kappa i}^S(r)$, respectively. Obtaining closed-form expressions for $J_{ij}^{L;\kappa}(q)$ and $J_{ij}^{S;\kappa}(q)$ expressions was not an easy task, and those formulas, along with their derivation, are presented in the Appendix. Additionally, elsewhere we have described a Fortran 90 computer program developed by us, which uses these expressions to compute the atomic CPs from a set of given Dirac orbitals expressed as a linear combination of KBGFs [20].

Here we would like to comment on possible quantitative manifestations of relativistic effects in Compton profiles. One obvious way to quantify the relativistic effects on the CPs is by comparing the values obtained from the DHF calculations with those obtained from nonrelativistic HF calculations. There is another way by which one can judge the influence of relativistic effects on Compton profiles, that is by comparing the orbital CPs of different fine-structure components. For example, in nonrelativistic calculations, np, nd,… orbitals have only one set of values each for the orbital CPs. However, in relativistic calculations, each such orbital splits into two fine-structure components, i.e., $np_{1/2}/np_{3/2}$, $nd_{3/2}/nd_{5/2}$, which, if the relativistic effects are strong, can differ from each other in a significant manner. Thus, one expects, that under such situations, the orbital profiles of the two fine-structure components will also be significantly different. Therefore, we will also examine this "fine-structure splitting" of the orbital CPs of various atoms to quantify the relativistic effects.

III. CALCULATIONS AND RESULTS

In this section we present our DHF results on the atomic profiles of the rare gases. The DHF orbitals of various atoms were computed using the KBGF-based REATOM code of Mohanty and Clementi [21]. During the DHF calculations the value of the speed of light used was $c=137.037$ a.u. Additionally, for obtaining the radius of the nucleus for the finite-nucleus approximation description of $V_{\text{nuc}}(r)$, values of atomic mass A were taken to be 4.026, 20.18, 39.948, 83.80, 131.3, and 222.0 for He, Ne, Ar, Kr, Xe, and Rn, respectively. Using the orbitals obtained from the DHF calculations, the atomic CPs were computed using our computer program COMPTON [20]. Next we present our results for the rare gas atoms, one by one. In order to investigate the basis-set dependence of the CPs, for each atom, two types of basis sets were used: (i) a large universal basis set proposed by Malli *et al.* [22] and (ii) a smaller basis set tailor made for the individual atom.

A. He

For He, DHF calculations were performed with (i) well-tempered basis set of Matsuoka and Huzinaga [23] employing 12s functions [23] and (ii) the universal basis set using 22s functions [22]. The computed CPs are plotted in Fig. 1 as a function of the momentum transfer q. The results of our calculations for some selected values of q are presented in Table I. For the sake of comparison, the same table also contains the nonrelativistic HF results of Clementi and Roetti [24], as well as the experimental results of Eisenberger and Reed [25]. Upon inspection of the table, the following trends

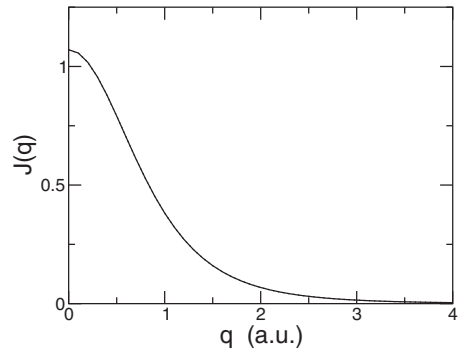

FIG. 1. DHF Compton profiles of He, $J(q)$, computed using the well-tempered basis set [23], and the universal basis set [22], as a function of the momentum transfer q. Profiles obtained using the two basis functions are virtually indistinguishable.

TABLE I. Relativistic (DHF) Compton profiles of He atom computed using various basis functions, compared to the nonrelativistic HF results [24] and the experiments [25].

q (a.u.)	$J(q)$ (WT)[a]	$J(q)$ (Uni)[b]	$J(q)$ (HF)[c]	$J(q)$ (Expt.)[d]
0.0	1.0704	1.0704	1.0705	1.071±1.5%
0.1	1.0567	1.0567	1.0568	1.058
0.2	1.0171	1.0171	1.017	1.019
0.3	0.9557	0.9557	0.955	0.958
0.4	0.8782	0.8782	0.878	0.881
0.5	0.7910	0.7910	0.791	0.795
0.6	0.7003	0.7004	0.700	0.705
0.7	0.6111	0.6112	0.611	0.616
0.8	0.5270	0.5270	0.527	0.533±2.3%
0.9	0.4503	0.4503	0.450	0.456
1.0	0.3820	0.3820	0.382	0.388
1.2	0.2712	0.2712	0.271	0.274
1.4	0.1910	0.1910	0.190	0.188
1.6	0.1344	0.1345	0.134	0.129
1.8	0.0952	0.0952	0.095	0.092
2.0	0.0678	0.0678	0.068	0.069
2.5	0.0307	0.0307	0.031	0.030±15%
3.0	0.0148	0.0148	0.015	0.013
5.0	0.0014	0.0014	—	—
8.0	0.0001	0.0001	—	—
10.0	0.00003	0.00003	—	—

[a]Our DHF results computed using the well-tempered (WT) basis set [23].
[b]Our DHF results computed using the universal basis set [22].
[c]Nonrelativistic HF results from Ref. [24].
[d]Experimental results from Ref. [25].

TABLE II. Relativistic (DHF) valence Compton profiles of Ne atom computed using various basis functions, compared to the nonrelativistic HF results [24] and the experiments [25].

q (a.u.)	$J(q)$ (WT)[a]	$J(q)$ (Uni)[b]	$J(q)$ (HF)[c]	$J(q)$ (Expt.)[d]	$J(q)$ (Expt.)[e]
0.0	2.5439	2.5452	2.548	2.582	2.602
0.1	2.5363	2.5375	2.540	2.574	2.593
0.2	2.5128	2.5140	2.515	2.558	2.560
0.3	2.4722	2.4731	2.475	2.519	2.506
0.4	2.4129	2.4133	2.418	2.451	2.435
0.5	2.3342	2.3339	2.335	2.359	2.340
0.6	2.2367	2.2357	2.236	2.249	2.235
0.7	2.1224	2.1210	2.120	2.124	2.099
0.8	1.9947	1.9933	1.990	1.986	1.966
0.9	1.8579	1.8568	1.855	1.839	1.826
1.0	1.7166	1.7159	1.715	1.685	1.690
1.2	1.4360	1.4361	1.435	1.394	1.417
1.4	1.1776	1.1780	1.171	1.140	1.171
1.6	0.9533	0.9537	0.951	0.921	0.975
1.8	0.7663	0.7665	0.766	0.749	—
2.0	0.6142	0.6144	0.619	0.608	—
2.5	0.3559	0.3558	0.355	0.355	—
3.0	0.2125	0.2123	0.212	0.225	—
3.5	0.1318	0.1319	0.132	0.156	—
4.0	0.0852	0.0853	0.085	0.102	—
5.0	0.0397	0.0397	0.040	0.041	—

[a]Our DHF results computed using the well-tempered basis set [23].
[b]Our DHF results computed using the universal basis set [22].
[c]Nonrelativistic HF results from Ref. [24].
[d]Experimental results from Ref. [26].
[e]Experimental results from Ref. [27].

emerge: (i) Our relativistic CPs computed with the well-tempered and the universal basis sets are in excellent agreement with each other. This implies that the smaller well-tempered basis set is virtually complete, as far as the CPs are concerned. (ii) Our DHF CPs are in excellent agreement with the nonrelativistic HF CPs of Clementi and Roetti [24]. This, obviously, is a consequence of the fact that the relativistic effects are negligible for a light atom such as He. (iii) Generally, the agreement between the theoretical and the experimental CPs is excellent, implying that the electron-correlation effects do not make a significant contribution in this case.

B. Ne

DHF calculations were performed for Ne using (i) $(14s,14p)$ well-tempered basis set of Matsuoka and Huzinaga [23] and (ii) the large $(32s,29p)$ universal basis set of Malli *et al.* [22]. In order to facilitate direct comparison with the experiments, the valence CPs (excluding the contribution from the $1s$ core orbital) obtained from our calculations are presented in Table II. They are also compared to the nonrelativistic HF results of Clementi and Roetti [24], the classic

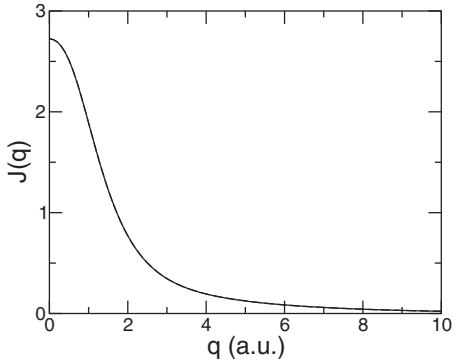

FIG. 2. DHF Compton profiles of Ne, $J(q)$, computed using the well-tempered basis set [23] and the universal basis set [22] as a function of the momentum transfer q. Profiles obtained using the two basis sets are virtually indistinguishable. All numbers are in atomic units.

experiment of Eisenberger [26], and more recent experiment of Lahmam-Bennani *et al.* [27]. Additionally, the total Compton profiles of Ne (including the contribution of the $1s$ orbital), computed using both the aforesaid basis sets, are plotted in Fig. 2.

Upon inspecting Table II we notice the following trends: (i) profiles computed using two different sets are again in very good agreement with each other, implying that both the basis sets are essentially complete and (ii) our relativistic profiles are in quite good agreement with the nonrelativistic HF profiles [24], essentially implying that even in Ne, the relativistic effects are quite negligible. As far as comparison with the experiments is concerned, for smaller values of q there is slight disagreement with the theory which progressively disappears as one approaches the large momentum-transfer regime. This suggests that electron-correlation effects possibly play an important role in the small momentum transfer regime.

Finally we examine the individual orbital CPs of the Ne atom in Fig. 3. The maximum contribution to the total CP for small values of momentum transfer comes from the $2s$ orbital, while in the same region, the smallest contribution comes from the $1s$ core orbital. The orbital CP of the $2s$

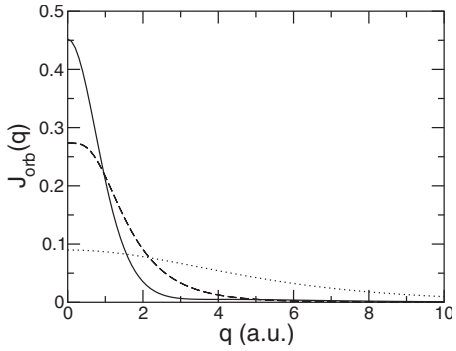

FIG. 3. Orbital Compton profiles of Ne for $2s$ (solid line), $2p_{3/2}/2p_{1/2}$ (dashed line), and $1s$ (dotted line), plotted with respect to q. Compton profiles of $2p_{1/2}$ and $2p_{3/2}$ orbitals are virtually indistinguishable. These profiles were computed using the universal basis set [22].

orbital varies rapidly with respect to q and becomes quite small for $q \geqslant 2$ a.u. On the other hand, the orbital profile of the $1s$ orbital shows the least dispersion with respect to q, and has the largest magnitude in the large q region, as compared to other orbital profiles. The behavior of the $2p_{1/2}/2p_{3/2}$ orbital profiles is intermediate as compared to the two extremes of $1s$ and $2s$ profiles. These profiles have lesser magnitude compared to the $2s$ profile for $q \approx 0$, while they vary more rapidly with respect to q, when compared to the $1s$ profile. Another pointer to the insignificance of the relativistic effects for Ne is the fact that the difference in the values of the $2p_{1/2}$ and $2p_{3/2}$ is quite small for all values of q.

C. Ar

Next, we discuss our calculated Compton profiles of Ar. The DHF calculations on Ar atom were performed using the following two basis sets: (i) smaller $(16s,16p)$ well-tempered basis set of Matsuoka and Huzinaga [23], and the (ii) large $(32s,29p)$ universal basis set of Malli *et al.* [22]. Calculated total CPs of Ar, for a selected number of q values in the range 0 a.u. $\leqslant q \leqslant$ 15 a.u., are presented in Table III. The same table also contains the nonrelativistic HF results of Clementi and Roetti [24], numerical-orbital-based DHF results of Mendelsohn *et al.* [14], and the experimental results of Eisenberger and Reed [25].

Additionally, in Figs. 4 and 5, respectively, we present our total and orbital CPs of Ar plotted as a function of the momentum transfer q. From Ar onwards, CP results of Mendelsohn *et al.* [14] exist, which were computed from the DHF orbitals obtained from finite-difference-based calculations. If our calculated CPs are correct, they should be in good agreements with those of Mendelsohn *et al.* [14]. Therefore, it is indeed heartening for us to note that our CP results computed with the universal basis set [22] are in perfect agreement with those of Mendelsohn *et al.* [14] to the decimal places, and for the q points, reported by them. As a matter of fact, even our CPs obtained using the smaller well-tempered basis set [23] disagree with those of Mendelsohn *et al.* [14] by very small amounts. Thus, this gives us confidence about the essential correctness of our approach.

When compared to the experiments, for $q=0$, our value of CP of 5.054 computed with universal basis set, is in excellent agreement with the experimental value of 5.058 [25]. For 0.1 a.u. $\leqslant q \leqslant$ 0.8 a.u., our results begin to overestimate the experimental ones slightly. For $q \geqslant 0.9$ a.u., however, our theoretical results underestimate the experimental results by small amounts. The nonrelativistic HF results [24] also exhibit the same pattern with respect to the experimental results. Upon comparing our CPs to the nonrelativistic HF CPs [24], we notice that the two sets of values differ slightly for smaller values of q. However, the difference between the two begins to become insignificant as we approach larger values of q, suggesting that the relativistic effects will be most prominent for $q \approx 0$.

Finally we examine the contributions of the individual orbitals to the atomic CP in Fig. 5, which presents the orbital profiles of all the orbitals of Ar. We observe the following trends: (i) $3s$ profile has the maximum value at $q=0$, followed by $3p_{3/2}/3p_{1/2}$ profiles. The minimum value at $q=0$ corresponds to the $1s$ profile. (ii) Profiles of outer orbitals vary more rapidly with q, as compared to the inner ones. In other words, profile flattening occurs as one moves inwards from the valence to the core orbitals. (iii) Again no significant fine-structure splitting is observed, in that the profiles of $np_{3/2}$ and $np_{1/2}$ orbitals differed from each other by small amounts, pointing to the smallness of relativistic effects.

TABLE III. Our relativistic (DHF) total Compton profiles of Ar atom computed using various basis sets, compared to the relativistic results of other authors [14], the nonrelativistic HF results [24], and the experiments [25].

q (a.u.)	$J(q)$ (WT)[a]	$J(q)$ (Uni)[b]	$J(q)$ (DHF)[c]	$J(q)$ (HF)[d]	$J(q)$ (Expt.)[e]
0.0	5.0471	5.0543	5.05	5.052	5.058±0.7%
0.1	5.0229	5.0302	5.03	5.028	5.022
0.2	4.9473	4.9539	4.95	4.950	4.917
0.3	4.8130	4.8171	—	4.812	4.749
0.4	4.6143	4.6144	4.61	4.608	4.526
0.5	4.3528	4.3487	—	4.369	4.259
0.6	4.0395	4.0324	4.03	4.028	3.960
0.7	3.6928	3.6854	—	3.690	3.643
0.8	3.3343	3.3288	—	3.328	3.319
0.9	2.9842	2.9814	—	2.982	3.000
1.0	2.6576	2.6573	2.66	2.658	2.697±1%
1.2	2.1071	2.1088	—	2.108	2.164
1.4	1.7011	1.7022	—	1.701	1.753
1.6	1.4163	1.4166	—	1.417	1.461
1.8	1.2198	1.2197	—	1.221	1.264
2.0	1.0825	1.0824	1.08	1.084	1.129
2.5	0.8728	0.8727	—	0.873	0.904
3.0	0.7360	0.7360	—	0.736	0.744
3.5	0.6216	0.6217	—	0.621	0.634
4.0	0.5207	0.5208	0.521	0.520	0.534±2.5%
7.0	0.1773	0.1774	—	0.177	0.181
8.0	0.1300	0.1300	—	0.130	0.137
9.0	0.0981	0.0981	—	0.098	0.104
10.0	0.0758	0.0757	0.076	0.075	0.078±10%
15.0	0.0254	0.0254	—	0.025	0.025

[a]Our DHF results computed using the well-tempered basis set [23].
[b]Our DHF results computed using the universal basis set [22].
[c]DHF results of Mendelsohn *et al.* [14] based upon finite-difference calculations.
[d]Nonrelativistic HF results from Ref. [24].
[e]Experimental results from Ref. [25].

D. Kr

Now, we discuss our DHF results of Compton profile of Kr. The DHF calculations on Kr atom were performed using the following two basis sets: (i) the smaller $(20s,15p,9d)$ basis set of Koga *et al.* [28] and (ii) the large $(32s,29p,20d)$ universal basis set of Malli *et al.* [22]. Calculated total CPs

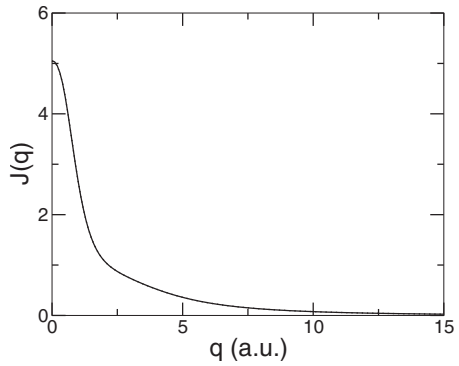

FIG. 4. DHF Compton profiles of Ar, $J(q)$, computed using the well-tempered basis set [23] and the universal basis set [22] as a function of the momentum transfer q. Profiles obtained using the two basis sets can be seen to differ slightly for $q \approx 0$.

of Kr, for 0 a.u. $\leqslant q \leqslant$ 30 a.u., are presented in Table IV, which also contains the nonrelativistic HF profiles computed by Clementi and Roetti [24], DHF profiles calculated by Mendelsohn *et al.* [14], and the experimental results of Eisenberger and Reed [25].

In Figs. 6 and 7, respectively, our total and orbital CPs of Kr are plotted as a function of the momentum transfer q. Upon comparing our CPs of Kr obtained using two basis sets we note that (i) for small values of q, the values obtained using the smaller basis set of Koga *et al.* [28] are slightly smaller than the ones obtained using the universal basis set and (ii) for large values of q, the results obtained using the two basis sets are in excellent agreement with each other. Next, we compare our calculated CPs with those computed by Mendelsohn *et al.* [14] using the numerical orbitals obtained in their DHF calculations. From Table IV it is obvious that, for the all the q values for which Mendelsohn *et al.* [14] reported their CPs, our profiles obtained using the universal basis set [22] are in exact agreement with their results. As a matter of fact, the agreement between the results of Mendelsohn *et al.* [14] and our results computed using the smaller basis set of Koga *et al.* [28] is also excellent.

Upon comparing our results to experimental ones, we see that our universal basis set value of $J(q=0)=7.187$ is in excellent agreement with the experimental value of 7.205 [25]. For other values of momentum transfer in the range 0.1 a.u. $\leqslant q \leqslant$ 1.0 a.u., although the agreement between our results and the experiments is slightly worse, our results are closer to the experimental value as compared to the nonrelativistic HF results [24]. For higher values of momentum transfer, our DHF results are fairly close to the HF results, suggesting that in the region of large q, relativistic effects are unimportant. Thus, we conclude that from Kr onwards, rela-

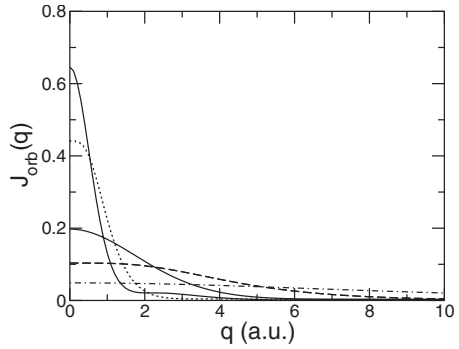

FIG. 5. Orbital Compton profiles of Ar, plotted as functions of the momentum transfer q. In the decreasing order of the value of $J_{\text{orb}}(q=0)$, the profiles correspond to $3s$, $3p_{3/2}/3p_{1/2}$, $2s$, $2p_{3/2}/2p_{1/2}$, and $1s$ orbitals. Note that for all the cases, profiles of $p_{3/2}$ and $p_{1/2}$ orbitals are virtually identical. These profiles were computed using the universal basis set [22].

TABLE IV. Our results on total profiles of Kr computed using the smaller basis set of Koga, Tatewaki, and Matsuoka (KTM) [28], and the universal basis set [22]. Relativistic results of other authors [14], nonrelativistic HF results [24], and the experimental results [25] are also presented for comparison.

q (a.u.)	$J(q)$ (KTM)[a]	$J(q)$ (Uni)[b]	$J(q)$ (DHF)[c]	$J(q)$ (HF)[d]	$J(q)$ (Expt.)[e]
0.0	7.1788	7.1871	7.19	7.228	7.205
0.1	7.1470	7.1548	7.15	7.194	7.152
0.2	7.0452	7.0505	7.05	7.085	7.022
0.3	6.8588	6.8595	—	6.888	6.767
0.4	6.5780	6.5735	6.57	6.595	6.459
0.5	6.2087	6.2010	—	6.216	6.098
0.6	5.7744	5.7670	5.77	5.776	5.701
0.7	5.3093	5.3053	—	5.309	5.289
0.8	4.8485	4.8486	—	4.848	4.880
0.9	4.4197	4.4225	—	4.420	4.491
1.0	4.0395	4.0429	4.04	4.039	4.133
1.2	3.4425	3.4432	—	3.441	3.540
1.4	3.0368	3.0353	—	3.037	3.122
1.6	2.7662	2.7650	—	2.769	2.850
1.8	2.5787	2.5785	—	2.583	2.670
2.0	2.4362	2.4364	2.44	2.441	2.533
2.5	2.1425	2.1428	—	2.144	2.219
3.0	1.8571	1.8572	—	1.857	1.898
3.5	1.5784	1.5782	—	1.578	1.597
4.0	1.3257	1.3255	1.33	1.326	1.338
5.0	0.9333	0.9335	—	0.934	0.937
6.0	0.6773	0.6773	0.677	0.678	0.683
7.0	0.5118	0.5118	—	0.512	0.522
8.0	0.4001	0.4001	—	0.400	0.399
9.0	0.3205	0.3205	—	0.319	0.316
10.0	0.2608	0.2608	0.261	0.259	0.254
15.0	0.1062	0.1062	—	0.104	0.095
20.0	0.0506	0.0506	—	0.049	0.044
25.0	0.0271	0.0271	0.027	0.026	0.022
30.0	0.0157	0.0157	—	0.015	0.009

[a]DHF results computed using the basis set of Koga, Tatewaki, and Matsuoka [28].
[b]DHF results computed using the universal basis set [22].
[c]DHF results of Mendelsohn *et al.*[14] based upon finite-difference calculations.
[d]Nonrelativistic HF results from Ref. [24].
[e]Experimental results from Ref. [25].

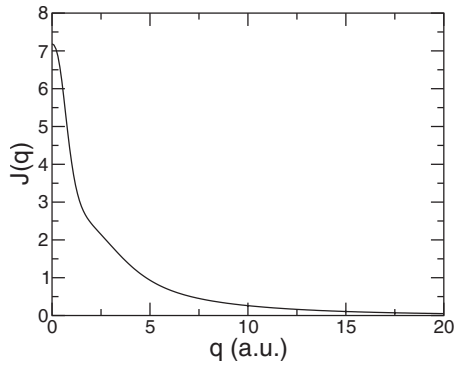

FIG. 6. DHF Compton profile of Kr, $J(q)$, computed using the universal basis set [22], plotted as a function of the momentum transfer q.

tivistic effects make their presence felt in the small q region.

Finally, we investigate the orbital CPs of Kr in Fig. 7, which presents the plots of the profiles of outer orbitals starting from $3d_{3/2}$ to $4p_{3/2}$. As far as the general trends of the orbital profiles are concerned, they are similar to what we observed for the cases of Ne and Ar, except for one important aspect. Unlike the Ne and Ar, for Kr we begin to observe the fine-structure splitting in the orbital profiles of $4p_{3/2}$ and $4p_{1/2}$ orbitals in the low q region, as is obvious from Fig. 7. For example, for $q=0$, corresponding values are $J_{4p_{3/2}}=0.508$ and $J_{4p_{1/2}}=0.496$, amounting to a difference of $\approx 2\%$. This is in complete agreement with our earlier observation that the relativistic effects make significant contributions to the CPs of Kr in the small q region.

E. Xe

In this section, we discuss our results on the relativistic Compton profiles of Xe. The DHF calculations on Xe atom were performed using the following two basis sets: (i) the smaller $(22s,18p,12d)$ basis set of Koga *et al.* [28] and (ii) the large $(32s,29p,20d)$ universal basis set of Malli *et al.* [22]. Total CPs of Xe, for selected values of momentum transfer in the range 0 a.u. $\leqslant q \leqslant$ 100 a.u., are presented in

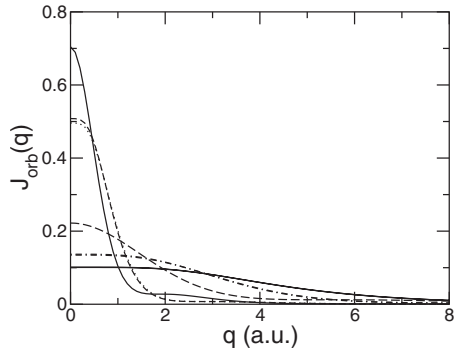

FIG. 7. Orbital Compton profiles of Kr for $4s$, $4p_{3/2}$, $4p_{1/2}$, $3s$, $3p_{3/2}/3p_{1/2}$, and $3d_{5/2}/3d_{3/2}$ orbitals in the order of decreasing values at $q=0$. For small q values, the differences between the $4p_{3/2}$ and $4p_{1/2}$ profiles are visible. These profiles were computed using the universal basis set [22].

TABLE V. Total CPs of Xe computed using the smaller basis set of Koga, Tatewaki, and Matsuoka (KTM) [28], and the universal basis set [22]. Relativistic results of other authors [14] and nonrelativistic HF results [14] are also presented for comparison.

q (a.u.)	$J(q)$ (KTM)[a]	$J(q)$ (Uni)[b]	$J(q)$ (DHF)[c]	$J(q)$ (HF)[d]
0.0	9.722	9.737	9.74	9.88
0.1	9.673	6.687	9.69	9.82
0.2	9.515	9.523	9.52	9.65
0.4	8.784	8.775	8.78	8.85
0.6	7.597	7.587	7.59	7.62
1.0	5.448	5.451	5.45	5.46
1.5	4.293	4.292	4.29	4.31
2.0	3.678	3.678	3.68	3.69
4.0	1.707	1.707	1.71	1.72
6.0	1.060	1.061	1.06	1.06
10.0	0.5150	0.5150	0.515	0.515
25.0	0.0660	0.0662	0.066	0.064
50.0	0.0088	0.0088	0.0088	0.0076
100.0	0.00067	0.0067	0.00068	0.00043

[a]Our DHF results computed using the basis set of Koga, Tatewaki, and Matsuoka [28].
[b]Our DHF results computed using the universal basis set [22].
[c]DHF results of Mendelsohn *et al.* [14] based upon finite-difference calculations.
[d]Nonrelativistic HF results reported in Ref. [14].

Table V. For the sake of comparison, the same table also contains DHF and the nonrelativistic HF profiles calculated by Mendelsohn *et al.* [14]. Here, we are unable to compare our results with the experiments because, to the best of our knowledge, no experimental measurements of the CPs of Xe exist.

Additionally, in Figs. 8 and 9, respectively, we present the plots of our total and orbital CPs of Xe. Upon comparing our total CPs obtained using the two basis sets we find that, as before, they disagree for smaller values of q, with the CPs obtained using the smaller basis set [28] being slightly lower than those obtained using the universal basis set [22]. As is obvious from Table V, that for $q \geqslant 1.5$ a.u., the two sets of basis functions yield virtually identical results. In the same

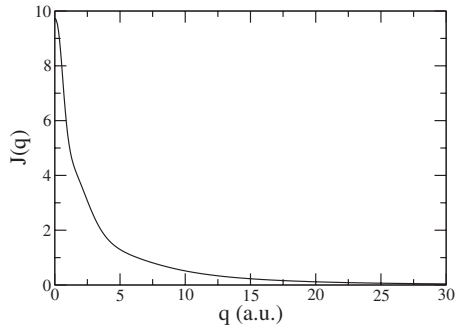

FIG. 8. DHF Compton profile of Xe, computed using the universal basis set [22] and plotted as a function of the momentum transfer q.

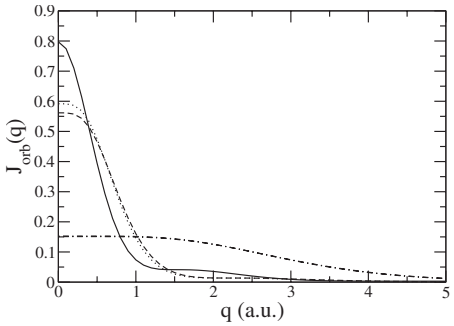

FIG. 9. Orbital Compton profiles of Xe for $5s$, $5p_{3/2}$, $5p_{1/2}$, and $4d_{5/2}/4d_{3/2}$ orbitals in the order of decreasing values at $q=0$. For small q values, the differences between the $5p_{3/2}$ and $5p_{1/2}$ profiles are quite significant. These profiles were computed using the universal basis set [22].

table, when we compare our results to the earlier DHF results of Mendelsohn *et al.* [14], we find that for all the q values, the agreement between our universal basis-set-based CPs, and their results, is perfect up to the decimal places reported by them. This again points to the correctness of our calculations.

Upon comparing our DHF results to the nonrelativistic HF results of Mendelsohn *et al.* [14], we find that for smaller values of q, the DHF values of CPs are smaller than the HF values, while for large values of q, the trend is just the opposite.

Finally, upon examining the orbital profiles presented in Fig. 9, we observe further evidence of the importance of relativistic effects in Xe. As is obvious from the figure, the fine-structure splitting between the orbitals profiles of $5p_{3/2}$ and $5p_{1/2}$ orbitals is larger as compared to $4p_{3/2}/4p_{1/2}$ splitting in Kr, and persists for a longer range of q values. For smaller values of q, $J_{5p_{3/2}}(q) > J_{5p_{1/2}}(q)$, while for large q values, the opposite is the case. For $q=0$, $J_{5p_{3/2}}=0.592$, while $J_{5p_{1/2}}=0.562$, which amounts to a difference of $\approx 5\%$.

F. Rn

As far as atomic Rn is concerned, to the best of our knowledge, no prior experimental studies of its Compton profiles exist. However, Biggs *et al.* [15] did perform DHF calculations of this atom, using a finite difference approach, with which we compare our results later on in this section. Our DHF calculations on Rn atom were performed using the following two basis sets: (i) the smaller $(25s,21p,15d,10f)$ basis set of Koga *et al.* [29] and (ii) the large $(32s,29p,20d,15f)$ universal basis set of Malli *et al.* [22]. Total CPs of Rn, for selected values of momentum transfer in the range 0 a.u. $\leqslant q \leqslant$ 100 a.u., are presented in Table VI.

Our results for total and orbital CPs of Rn are plotted in Figs. 10 and 11, respectively. As for other atoms, we find that our total CPs obtained using the two basis sets disagree for smaller values of q, with the CPs obtained using the smaller basis set of Koga *et al.* [29] being slightly smaller than those obtained using the universal basis set [22]. From Table VI we deduce that for $q \geqslant 4.0$ a.u., the two sets of basis functions yield virtually identical values of CPs. In the same table,

TABLE VI. Total CPs of Rn computed using the smaller basis set of Koga, Tatewaki, and Matsuoka (KTM) [29] and the universal basis set [22], compared to the earlier calculations of Biggs *et al.* [15].

q (a.u.)	$J(q)$ (KTM)[a]	$J(q)$ (Uni)[b]	$J(q)$ (DHF)[c]
0.0	11.8344	11.8531	11.9
0.1	11.7850	11.8026	11.8
0.2	11.6176	11.6306	11.6
0.4	10.8055	10.7996	10.8
0.6	9.4877	9.4744	9.47
1.0	7.2130	7.2130	7.21
1.6	5.8127	5.8132	5.81
2.0	5.1530	5.1533	5.15
4.0	2.8379	2.8381	2.84
6.0	2.0453	2.0454	2.05
10.0	0.9804	0.9804	0.98
30.0	0.1083	0.1083	0.11
60.0	0.0166	0.0166	0.017
100.0	0.0037	0.0037	0.0037

[a]Our DHF results computed using the basis set of Koga, Tatewaki, and Matsuoka [29].
[b]Our DHF results computed using the universal basis set [22].
[c]DHF results of Biggs *et al.* [15] based upon finite-difference calculations.

when we compare our results to the earlier DHF calculations of Biggs *et al.* [15], we find that for all the q values, the agreement between our universal basis-set-based CPs and their results is perfect up to the decimal places reported by them.

Of all the rare gas atoms considered so far, on the intuitive grounds we expect the relativistic effects to be the strongest in Rn. Indeed, this is what we confirm upon investigating the orbital profiles presented in Fig. 11. As is obvious from the figure, the splitting between the orbitals profiles of $6p_{3/2}$ and $6p_{1/2}$ orbitals is quite big, and persists for a large range of q values. Similar to the case of Xe, here also for smaller values of q, $J_{6p_{3/2}}(q) > J_{6p_{1/2}}(q)$, while for large q values, opposite is the case. For $q=0$, $J_{6p_{3/2}}=0.644$, while $J_{6p_{1/2}}=0.551$, amounting to a difference of $\approx 15\%$, which is quite substantial. The

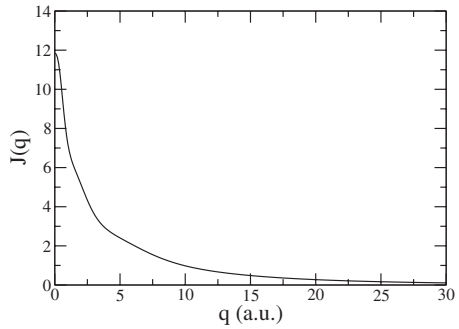

FIG. 10. DHF Compton profile of Rn, computed using the universal basis set [22] and plotted as a function of the momentum transfer q.

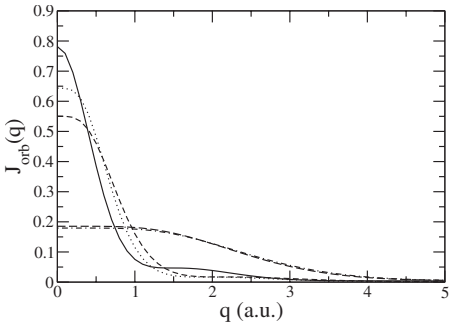

FIG. 11. Orbital Compton profiles of Rn for $6s$, $6p_{3/2}$, $6p_{1/2}$, and $5d_{5/2}/5d_{3/2}$ orbitals in the order of decreasing values at $q=0$. For small q values, the differences between the $6p_{3/2}$ and $6p_{1/2}$ profiles are quite large. Even the splitting of $5d_{5/2}$ and $5d_{3/2}$ profiles is visible. These profiles were computed using the universal basis set [22].

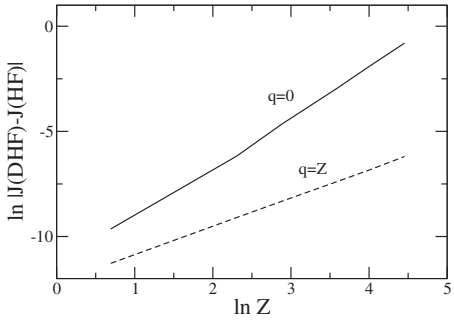

FIG. 12. Difference between the relativistic (J(DHF)) and the nonrelativistic (J(HF)) Compton profiles plotted, on a logarithmic scale, as a function of the atomic number Z. Plots correspond to the momentum transfer values $q=0$ and $q=Z$.

fine-structure splitting between the profiles of $5d_{5/2}$ and $5d_{3/2}$ orbitals although is not quite that large, yet it is visible in Fig. 11. At $q=0$, $J_{5d_{5/2}}=0.185$ and $J_{5d_{3/2}}=0.179$, leading to a difference of $\approx 3\%$, which is quite significant for an inner orbital. Thus, we conclude that the relativistic effects are quite substantial in case of Rn, and, therefore, it will be useful if experiments are performed on this system to ascertain this.

G. Z dependence of relativistic effects on Compton profiles

In earlier sections, while discussing relativistic effects on Compton profiles, we noticed that they were most prominent for small momentum transfers. Moreover, one intuitively expects the relativistic effects to increase with increasing atomic number Z. In this section our aim is to perform a quantitative investigation of relativistic effects on quantum profiles, as a function of Z, for both large and small values of momentum transfer. We noticed that for small momentum transfers, DHF values of J were smaller than their nonrelativistic counterparts, while for large momentum transfer opposite was the case. Therefore, for a given value of momentum transfer q, we quantify relativistic effects in terms of $|J(\mathrm{DHF})-J(\mathrm{HF})|$, which is the magnitude of the difference of relativistic DHF value of the Compton profile (J(DHF)), and the nonrelativistic HF value of the profile (J(HF)). We obtain J(HF) by using a large value of the velocity of light ($c=10^4$ a.u.) in the DHF calculations. We explore the dependence of this quantity on Z, for two values of momentum transfer, $q=0$ and $q=Z$ a.u., where the latter value clearly belongs to the large momentum transfer regime. The values of $\ln|J(\mathrm{DHF})-J(\mathrm{HF})|$ as a function of $\ln Z$, are presented in Fig. 12 for both these values of momentum transfer. From the figure it obvious that, to a very good approximation, the corresponding curves are straight lines, suggesting a power-law dependence of the relativistic effects on Z. The slopes of the least-square-fit line for $q=0$ is 2.36 while for $q=Z$, the slope is 1.35. Of course, these results are based upon data points generated by six values of Z (rare gas series), and consequently can only be treated as suggestive. But the results suggest (i) super-linear dependence of the relativistic effect on quantum profiles in both momentum transfer regimes, and (ii) stronger influence of relativity in the small momentum transfer regime as compared to the large one. Of course, this exploration can be refined further by separately investigating the Z dependence of these effects on the core and valence profiles. Additionally, this investigation can be extended to a larger number of atoms to obtain a larger set of data points. However, these calculations are beyond the scope of the present work and will be presented elsewhere.

IV. CONCLUSIONS AND FUTURE DIRECTIONS

In this paper, we presented an approach aimed at computing the relativistic Compton profiles of atoms within the DHF approximation, when the atomic orbitals are represented as linear combinations of kinetically balanced set of Gaussian functions. The approach was applied to compute the CPs of rare gas atoms ranging from He to Rn, and results were compared to the experimental profiles, and theoretical profiles of other authors, wherever such data was available. Additionally, the influence of size and type of basis set was examined by performing calculations on each atom with two basis sets: (i) a well-known smaller basis set and (ii) a large universal basis set proposed by Malli *et al.* [22].

Upon comparing our results with the experiments, we found that for lighter atoms He, Ne, and Ar, the agreement was similar to what one obtains from the nonrelativistic HF calculations, indicating lack of any significant relativistic effects for these atoms. For Kr, we noticed that for smaller momentum transfer values, DHF results were in better agreement with the experiments, as compared to the HF results. For heavier atoms, Xe and Rn, unfortunately no experimental data is available. Yet another quantitative indicator of the importance of relativistic effects is the fine-structure splitting of the profiles, i.e., the difference in the profiles of $np_{1/2}/np_{3/2}$, etc., which will have identical profiles in nonrelativistic calculations. We found that this splitting becomes larger with the increasing atomic number of the atom, thus justifying a relativistic treatment of the problem for heavy atoms. Additionally, by comparing our results with the nonrelativistic HF results we found that the relativistic effects are most prominent in the region of small momentum transfer, while at large momentum transfer, their contribution is much smaller.

In the literature, we were able to locate prior theoretical calculation of relativistic CPs of atoms only from one group, namely the DHF calculations of Mendelsohn *et al.* [14] and Biggs *et al.* [15], performed on Ar, Kr, Xe, and Rn, employing a finite-difference-based approach. The CPs computed by them [14,15] for these atoms were found to be in perfect agreement with our results computed using the universal basis set. This testifies to the correctness of our approach, and suggests that by using a large basis set it is possible to reach the accuracy of finite-difference approaches in relativistic calculations, not just on total energies [22] but also on expectation values.

Having investigated the influence of the relativistic effects, the next logical step will be to go beyond the mean-field DHF treatment and incorporate the influence of electron correlations on atomic CPs within a relativistic framework. Such a treatment can be within a relativistic CI framework [9], or can also be performed within a perturbation-theoretic formalism. Work along these lines is currently underway in our group and the results will be submitted for publication in the future.

APPENDIX A: A DERIVATION OF COMPTON PROFILE MATRIX ELEMENTS OVER KINETICALLY BALANCED GAUSSIAN BASIS SETS

During our discussion here we use the same notations for various quantities as adopted in Sec. II. Our aim here is to evaluate the closed form expressions for the following two integrals:

$$J_{ij}^{L;\kappa}(q) = \frac{1}{2}\int_q^\infty p g_{\kappa i}^L(p) g_{\kappa j}^L(p) dp, \tag{A1}$$

$$J_{ij}^{S;\kappa}(q) = \frac{1}{2}\int_q^\infty p g_{\kappa i}^S(p) g_{\kappa j}^S(p) dp, \tag{A2}$$

which, as explained in Sec. II, are needed to compute the orbital (and total) atomic CPs when the KBGF based numerical formalism is employed to solve the DHF equations. First, we will obtain expressions for $g_{\kappa i}^L(p)$ and $g_{\kappa i}^S(p)$, the radial Fourier transforms of the large and small component basis functions $g_{\kappa i}^L(r)$ and $g_{\kappa i}^S(r)$, respectively, defined as

$$g_{\kappa i}^L(p) = \frac{4\pi}{(2\pi)^{3/2}}\int_0^\infty r g_{\kappa i}^L(r) j_{l_A}(pr) dr, \tag{A3}$$

$$g_{\kappa i}^S(p) = \frac{4\pi}{(2\pi)^{3/2}}\int_0^\infty r g_{\kappa i}^S(r) j_{l_B}(pr) dr, \tag{A4}$$

where $j_{l_A}(pr)/j_{l_A}(pr)$ refer to the spherical Bessel functions corresponding to the orbital angular momentum l_A/l_B of the large and/or small component. The spherical Bessel function is related to the Bessel function by the well-known relation

$$j_\nu(x) = \sqrt{\frac{\pi}{2x}} J_{\nu+1/2}(x), \tag{A5}$$

where $J_\nu(x)$ is the Bessel function.

1. Derivation for the large component

First, we obtain and expression for $g_{\kappa i}^L(p)$ by performing the integral involved in Eq. (A3). Substituting the expression for $g_{\kappa i}^L(r)$ from Eq. (3) into Eq. (A3), we obtain

$$g_{\kappa i}^L(p) = \frac{4\pi}{(2\pi)^{3/2}}\int_0^\infty N_{\kappa i}^L r^{(n_\kappa+1)} e^{-\alpha_i r^2} j_{l_A}(pr) dr$$

$$= \frac{N_{\kappa i}^L}{\sqrt{p}}\int_0^\infty N_{\kappa i}^L r^{(n_\kappa+1/2)} e^{-\alpha_i r^2} J_{l_A+1/2}(pr) dr, \tag{A6}$$

where in the last step, we have used Eq. (A5). Next, on using the relation $n_\kappa = l_A + 1$, and the definite integral [30]

$$\int_0^\infty x^{\nu+1} e^{-\alpha r^2} J_\nu(\beta x) dx$$

$$= \frac{\beta^\nu}{(2\alpha)^{\nu+1}} e^{-\beta^2/4\alpha} [\mathrm{Re}(\alpha) > 0, \mathrm{Re}(\nu) > 0], \tag{A7}$$

Eq. (A6) simplifies to

$$g_{\kappa i}^L(p) = N_{\kappa i}^L \frac{p^{l_A}}{(2\alpha_i)^{l_A+3/2}} e^{-p^2/4\alpha_i}. \tag{A8}$$

On substituting the above result in Eq. (A1), one obtains

$$J_{ij}^{L;\kappa}(q) = \frac{1}{2}\int_q^\infty (N_{\kappa i}^L)(N_{\kappa j}^L) \frac{p^{2l_A+1}}{(4\alpha_i\alpha_j)^{l_A+3/2}} e^{-p^2/4\alpha_{ij}} dp,$$

where $\alpha_{ij} = \frac{\alpha_i\alpha_j}{\alpha_i+\alpha_j}$. Next, on making the change of variable $t = \frac{p^2}{4\alpha_{ij}}$ in the integral above, leading to the lower limit $q_t = \frac{q^2}{4\alpha_{ij}}$, we obtain

$$J_{ij}^{L;\kappa}(q) = \frac{(N_{\kappa i}^L)(N_{\kappa j}^L)}{4} \frac{(4\alpha_{ij})^{l_A+1}}{(4\alpha_i\alpha_j)^{l_A+3/2}} \int_{q_t}^\infty t^{l_A} e^{-t} dt,$$

leading to the final expression

$$J_{ij}^{L;\kappa}(q) = \frac{(N_{\kappa i}^L)(N_{\kappa j}^L)}{4} \frac{(4\alpha_{ij})^{l_A+1}}{(4\alpha_i\alpha_j)^{l_A+3/2}} \Gamma(l_A+1, q_t), \tag{A9}$$

where $\Gamma(l_A+1, q_t)$ is the incomplete Γ function. Since l_A is a non-negative integer, the incomplete Γ function can be easily computed using the series [30]

$$\Gamma(l_A+1, q_t) = (l_A)! e^{-q_t} \sum_{m=0}^{l_A} \frac{q_t^m}{m!}. \tag{A10}$$

We note that our general result for $J_{ij}^{L;\kappa}(q)$ in Eq. (A9) leads to the same formulas as reported by Naon *et al.* [31] for the atomic CP matrix elements for *s*- and *p*-type Gaussian orbitals for the nonrelativistic case.

2. Derivation for the small component

We note that the explicit form of the small component basis function $g_{\kappa i}^S(r)$ [cf. Eq. (4)] is

$$g_{\kappa i}^S(r) = N_{\kappa i}^S N_{\kappa i}^L [(n_\kappa + \kappa) r^{n_\kappa - 1} e^{-\alpha_i r^2} - 2\alpha_i r^{n_\kappa+1} e^{-\alpha_i r^2}].$$

On substituting the above in Eq. (A4), the Fourier transform of the small component basis function becomes

TABLE VII. Relationship between quantum numbers κ, n_κ, and l_B, for relativistic atomic orbitals.

κ	n_κ	l_B
$-\left(j+\frac{1}{2}\right)$	$-\kappa$	$j+\frac{1}{2}=-\kappa$
$\left(j+\frac{1}{2}\right)$	$\kappa+1$	$j-\frac{1}{2}=\kappa-1$

$$g^S_{\kappa i}(p)=\frac{N^S_{\kappa i}N^L_{\kappa i}}{\sqrt{p}}\int_0^\infty [(n_\kappa+\kappa)r^{(n_\kappa-1/2)}-2\alpha_i r^{(n_\kappa+3/2)}] \times e^{-\alpha_i r^2}J_{l_B+1/2}(pr)dr. \tag{A11}$$

As before, we seek a relation between n_κ and l_B, which is summarized in Table VII. Here, the two cases have to be dealt with separately since the relations are different for the two possibilities.

a. Case (i): $\kappa=-(j+1/2)$

From Table VII it is easy to see that for this case $n_\kappa=l_B=-\kappa$. The integral in Eq. (A11) becomes

$$g^S_{\kappa i}(p)=\frac{N^S_{\kappa i}N^L_{\kappa i}}{\sqrt{p}}\int_0^\infty (-2\alpha_i)r^{(n_\kappa+3/2)}e^{-\alpha_i r^2}J_{n_\kappa+1/2}(pr)dr$$
$$=-N^S_{\kappa i}N^L_{\kappa i}\frac{p^{n_\kappa}}{(2\alpha_i)^{(n_\kappa+1/2)}}e^{-p^2/4\alpha_i}. \tag{A12}$$

b. Case (ii): $\kappa=(j+1/2)$

For this case, $l_B=n_\kappa-2=\kappa-1$, which upon substitution in Eq. (A11) yields

$$g^S_{\kappa i}(p)=\frac{N^S_{\kappa i}N^L_{\kappa i}}{\sqrt{p}}\int_0^\infty [(2n_\kappa-1)r^{(n_\kappa-1/2)}-2\alpha_i r^{(n_\kappa+3/2)}] \times e^{-\alpha_i r^2}J_{n_\kappa-3/2}(pr)dr. \tag{A13}$$

Next we use the result [30]

$$\int_0^\infty x^\mu e^{-\alpha x^2}J_\nu(\beta x)dx$$
$$=\frac{\beta^\nu\Gamma\left(\frac{\nu}{2}+\frac{\mu}{2}+\frac{1}{2}\right)}{2^{\nu+1}\alpha^{1/2(\mu+\nu+1)}\Gamma(\nu+1)}\Phi\left(\frac{\nu+\mu+1}{2},\nu+1,-\frac{\beta^2}{4\alpha}\right)$$
$$\text{for } \mathrm{Re}(\alpha)>0,\quad \mathrm{Re}(\mu+\nu)>-1, \tag{A14}$$

where $\Phi(a,b,z)$ is the confluent hypergeometric function in Eq. (A13), and after some simplifications obtain

$$g^S_{\kappa i}(p)=\frac{N^S_{\kappa i}N^L_{\kappa i}}{\sqrt{p}}\frac{p^{(n_\kappa-3/2)}}{2^{(n_\kappa-3/2)}\alpha_i^{(n_\kappa-1/2)}}\left[\left(n_\kappa-\frac{1}{2}\right)\Phi\left(n_\kappa-\frac{1}{2},n_\kappa-\frac{1}{2},-\frac{p^2}{4\alpha_i}\right)-\left(n_\kappa-\frac{1}{2}\right)\Phi\left(n_\kappa+\frac{1}{2},n_\kappa-\frac{1}{2},-\frac{p^2}{4\alpha_i}\right)\right] \tag{A15}$$

Next, we use the following two identities involving the confluent hypergeometric functions [30]:

$$a\Phi(a+1,b,z)=(z+2a-b)\Phi(a,b,z)+(b-a)\Phi(a-1,b,z), \tag{A16}$$

$$\Phi(a,a,z)=e^z, \tag{A17}$$

to obtain the following simple expression from Eq. (A15),

$$g^S_{\kappa i}(p)=N^S_{\kappa i}N^L_{\kappa i}\frac{p^{n_\kappa}}{(2\alpha_i)^{(n_\kappa+1/2)}}e^{-p^2/4\alpha_i}. \tag{A18}$$

Comparing the results of the two cases (A12) and (A18), we find that they only differ by a sign, and hence when substituted in the expression for $J^{S;\kappa}_{ij}(q)$ in Eq. (A2) yield the same result

$$J^{S;\kappa}_{ij}(q)=\frac{1}{2}\int_q^\infty (N^S_{\kappa i})(N^S_{\kappa j})(N^L_{\kappa i})(N^L_{\kappa j})\frac{p^{2n_\kappa+1}}{(4\alpha_i\alpha_j)^{n_\kappa+1/2}}e^{-p^2/4\alpha_{ij}}dp,$$

where $\alpha_{ij}=\frac{\alpha_i\alpha_j}{\alpha_i+\alpha_j}$. The above integral can be evaluated in exactly the same way as was done before for the large component [cf. Eq. (A9)], to yield the final expression for the Compton profile matrix element

$$J^{S;\kappa}_{ij}(q)=\frac{(N^S_{\kappa i})(N^S_{\kappa j})(N^L_{\kappa}i)(N^L_{\kappa j})}{4}\frac{(4\alpha_{ij})^{l_A+2}}{(4\alpha_i\alpha_j)^{l_A+3/2}}\Gamma(l_A+2,q_t), \tag{A19}$$

where $q_t=\frac{q^2}{4\alpha_{ij}}$ and the incomplete Γ function is defined in Eq. (A10). Finally, the large and small components of the CP of an orbital can be computed in terms of these matrix elements as

$$J^L_{n\kappa}(q)=\sum_{i,j}C^L_{\kappa i}C^L_{\kappa j}J^{L;\kappa}_{ij}, \tag{A20}$$

$$J^S_{n\kappa}(q)=\sum_{i,j}C^S_{\kappa i}C^S_{\kappa j}J^{S;\kappa}_{ij}. \tag{A21}$$

It is these formulas derived here which have been numerically implemented in our computer program COMPTON [20] aimed at calculating relativistic atomic CPs.

[1] For a review see I. P. Grant, in *Methods in Computational Chemistry*, edited by S. Wilson (Plenum, New York, 1988), Vol. 12, p. 1.
[2] Y. K. Kim, Phys. Rev. **154**, 17 (1967).
[3] T. Kagawa, Phys. Rev. A **12**, 2245 (1975).
[4] Y. Ishikawa, R. C. Binning, and K. M. Sando, Chem. Phys. Lett. **101**, 111 (1983).
[5] K. G. Dyall, I. P. Grant, and S. Wilson, J. Phys. B **17**, 493 (1984).
[6] R. E. Stanton and S. Havriliak, J. Chem. Phys. **81**, 1910 (1984).
[7] A. K. Mohanty and E. Clementi, Chem. Phys. Lett. **157**, 348 (1989); J. Chem. Phys. **93**, 1829 (1990).
[8] O. Visser, L. Visscher, P. J. C. Aerts, and W. C. Nieuwpoort, Theor. Chim. Acta **81**, 405 (1992); O. Matsuoka, L. Pisani, and E. Clementi, Chem. Phys. Lett. **20**, 13 (1993); F. A. Parpia and A. K. Mohanty, Phys. Rev. A **52**, 962 (1995); A. K. Mohanty and F. A. Parpia, *ibid.* **54**, 2863 (1996).
[9] A. Shukla, M. Dolg, H.-J. Flad, A. Banerjee, and A. K. Mohanty, Phys. Rev. A **55**, 3433 (1997).
[10] L. Visscher, O. Visser, P. J. C. Aerts, H. Merenga, and W. C. Nieuwpoort, Comput. Phys. Commun. **81**, 120 (1994); Y. Watanabe and O. Matsuoka, J. Chem. Phys. **116**, 9585 (2002).
[11] For a review see *Compton Scattering*, edited by B. G. Williams (McGraw Hill, London, Great Britain, 1977).
[12] A. Shukla, M. Dolg, P. Fulde, and H. Stoll, Phys. Rev. B **57**, 1471 (1998).
[13] For a review of inelastic photon scattering from the inner-shell electrons, see P. P. Kane, Phys. Rep. **218**, 67 (1992).
[14] L. B. Mendelsohn, F. Biggs, and J. B. Mann, Chem. Phys. Lett. **26**, 521 (1974).
[15] F. Biggs, L. B. Mendelsohn, and J. B. Mann, At. Data Nucl. Data Tables **16**, 201 (1975).
[16] R. Ribberfors, Phys. Rev. B **12**, 2067 (1975).
[17] P. Holm, Phys. Rev. A **37**, 3706 (1988).
[18] P. M. Bergstrom, Jr., T. Surić, K. Pisk, and R. H. Pratt, Phys. Rev. A **48**, 1134 (1993).
[19] P. Eisenberger and P. M. Platzman, Phys. Rev. A **2**, 415 (1970).
[20] P. Jaiswal and A. Shukla, computer program COMPTON (unpublished).
[21] A. K. Mohanty and E. Clementi, in *Modern Techniques in Computational Chemistry*, edited by E. Clementi (ESCOM, Leiden, 1989), p. 169; also see the work of Mohanty and Clementi in Ref. [7].
[22] G. L. Malli, A. B. F. Da Silva, and Y. Ishikawa, Phys. Rev. A **47**, 143 (1993).
[23] O. Matsuoka and S. Huzinaga, Chem. Phys. Lett. **140**, 567 (1987).
[24] E. Clemenit and C. Roetti, At. Data Nucl. Data Tables **14**, 177 (1974).
[25] P. Eisenberger and W. A. Reed, Phys. Rev. A **5**, 2085 (1972).
[26] P. Eisenberger, Phys. Rev. A **5**, 628 (1972).
[27] A. Lahmam-Bennani, A. Duguet, and M. Rouault, J. Chem. Phys. **78**, 1838 (1983).
[28] T. Koga, H. Tatewaki, and O. Matsuoka, J. Chem. Phys. **115**, 3561 (2001).
[29] T. Koga, H. Tatewaki, and O. Matsuoka, J. Chem. Phys. **119**, 1279 (2003).
[30] *Handbook of Mathematical Functions with Formulas, Graphs, and Mathematical Tables*, edited by M. Abramowitz and I. A. Stegun (Dover, New York, 1965).
[31] M. Naon, M. Cornille, and M. Roux, J. Phys. B **4**, 1593 (1971).